Journal of Nuclear Materials 404 (2010) 165–173

Contents lists available at ScienceDirect

Journal of Nuclear Materials

journal homepage: www.elsevier.com/locate/jnucmat

Formation of helium induced nanostructure 'fuzz' on various tungsten grades

M.J. Baldwin *, R.P. Doerner

Center for Energy Research & Department of Mechanical and Aerospace Engineering, University of California–San Diego, 9500 Gilman Dr., La Jolla, CA 92093-0417, USA

ARTICLE INFO

Article history:
Received 19 March 2010
Accepted 25 June 2010

ABSTRACT

The response of a variety of W material grades to nanostructure 'fuzz' formation is explored. W targets are exposed to He or D_2–0.2He plasmas in PISCES-B at 900–1320 K to below sputter threshold He^+ ions of energy 25–60 eV for up to 2.2×10^4 s. SEM and XPS reveal nanoscopic reorganization of the W surface to a layer of 'fuzz' of porosity ~90% as determined by a 'fuzz' removal/weight loss method. The variability of 'fuzz' growth is examined at 1120 K for 1 h durations: SR, SC and doped W grades – La_2O_3 (1% wt.), Re (5% and 10% wt.), and TiC (1.5% wt.) developed 2–3 μm thick 'fuzz' layers, while a VPS grade developed a layer 4 μm thick. An RC grade revealed additional 'fuzz' at deep (>100 μm) grain boundaries. However, heat treatment up to 1900 K produced reintegration of 'fuzz' with the bulk and He release at ~1000 K and ~1400–1800 K due to depopulation from vacancy complexes.

1. Introduction

There is a widely held view that future burning-plasma devices will be engineered with tungsten or tungsten-alloy first-walls and plasma-facing components (PFC's). Tungsten has a high melting point (3695 K), excellent resistance to physical sputtering in detached plasma regimes [1], and most importantly, exhibits low in-bulk [2], and co-deposit [3] retention at elevated temperature. A further high temperature advantage is that neutron effects can 'heal' to an extent, as displacement damage migrates to grain boundaries more efficiently with increasing temperature [4]. Such potential benefits have recently led to alterations in the ITER-divertor design during the D–T operational phase, whereby the graphite divertor is to be fully replaced with W cassettes. This change will see W surfaces operated at a considerably higher ambient temperature, ~900 K at the vertical targets, compared with the previous design, where W usage was limited to the baffles and dome and to be operated at or below 600 K. The successful use of W in ITER will also pave the way for W usage in the future DEMO reactor, to be operated at an even higher ambient temperature, ~1000 K or above, in order to facilitate efficient heat-removal [1] and energy-extraction (e.g. Ref. [5]).

The drawback with tungsten edge materials however, is that as an eroded 'high-Z' impurity, it will seriously degrade reactor performance if even minute levels reach the core plasma [6]. Thus, for W to be compatible with fusion-reactor design, sputtering, ablation during high heat/particle load events, and dust production, must be kept minimal. Nevertheless, in spite of W having low-erosive yield, the progression in reactor technology toward continuous operation and higher first-wall temperature, has led to the observation of new issues surrounding the He–W interaction. Exposure of W to energetic He with plasmas and ions beams has been studied extensively and is well known for a multitude of He-induced-materials effects. Blistering can be observed at temperatures below 1000 K [7,8], but at higher temperature (>1000 K) the formation of pits, holes and bubbles [9–11] and nano [12–17] and microscale [7,18] surface structuring is found. In the temperature range expected for W PFCs in ITER and DEMO, considerable experimental evidence exists that shows He inclusion into the W surface leads to gross modification of the near surface W matrix into fragile nanoscopic structures [12–17]. The effect is typically observed on W surfaces of elevated temperature ($T \sim 1000$ K) exposed in steady state plasma devices ($t_{exp} > 10^2$ s) to large He ion fluxes (>10^{21} He^+ m^{-2} s^{-1}). Yet there are few, if any, convincing reports for its observation in present day fusion devices with W walls or limiters (e.g. ASDEX, LHD and TEXTOR) in spite of the formation conditions being relevant to the fusion first-wall regime. Although, it should be remarked for current devices, that the effect is not likely to proceed efficiently since only some of the required formation conditions are usually met simultaneously and/or plasma exposure time is too short.

W-nanostructure growth in a fusion device could potentially present a source of fragile, easily removed W at the plasma edge. The potential for surface exfoliation, modified erosion properties, reduced-thermal performance and impact on hydrogen isotope retention are naturally all currently open issues that, in turn, may adversely influence reactor performance and operation. Consequently, as these issues are relevant to W divertor operation in ITER, the He–W interaction has increasingly become the subject of ITER-divertor research and development activity. In this article, we expand on previous research [12,15–17] by reporting on

* Corresponding author. Tel.: +1 858 534 1655; fax: +1 858 534 7716.
E-mail address: mbaldwin@ferp.ucsd.edu (M.J. Baldwin).

0022-3115/$ - see front matter © 2010 Elsevier B.V. All rights reserved.
doi:10.1016/j.jnucmat.2010.06.034

further observations of He-induced effects on W at ITER and DEMO relevant temperatures. Properties of He-induced-nanostructured layers, the influence of surface temperature on nanostructure growth, and the nature of the effect on a range of different types of W relevant to use in a fusion device, are reported.

2. Experimental procedures

In the experiments reported here, the effects of a wide variety of He and mixed D_2–He plasma exposure conditions on a total of 24 W and W-alloy grade target specimens are explored. To maintain clarity only a brief summary of all of the experimental conditions is given here and specific experimental details are quoted where necessary. The collection of target specimens consisted of 19 pure W, 4 doped (Re, La_2O_3, TiC) W-alloy targets (25 mm dia. and 1.5 mm thick), and 1 W single crystal (8 mm dia. and 1 mm thick) fabricated by the floating-zone-melting method. Targets specimens were exposed to either He or D_2–0.2He mixture plasmas in the PISCES-B linear-divertor-plasma simulator (as in Ref. [15]). All of the targets were exposed to plasma such that the target temperature was maintained at a fixed value in the range 900–1320 K, for fixed time durations in the span 300–2.2×10^4 s.

During each exposure, the plasma conditions at the target location were measured using a reciprocating double Langmuir probe. Exposure plasmas (He or D_2–0.2He) of typical density, $n_e \sim 2$–6×10^{18} m^{-3}, and temperature, $T_e \sim 6$–8 eV were used. The typical He ion flux on target, for a pure He plasma was $\sim 5 \times 10^{22}$ ions m^{-2} s^{-1} and for D_2–0.2He mixture plasma, $\sim 1 \times 10^{22}$ ions m^{-2} s^{-1}. Targets were biased in the range −(40–75) V to facilitate energetic-ion bombardment. The energy of impacting ions can be estimated from the target bias, $\langle E_{ions} \rangle \approx V_{bias} - 2\,kT_e$.

Prior to, and following plasma exposure, targets were weighed on a microbalance to determine mass change. A measure of weight loss in this procedure facilitated study of erosion and/or mechanical stability of formed nanostructure surfaces. Further quantification of the modified nanostructure-surface layer was undertaken using cross-sectional scanning-electron microscopy (SEM). Cross-sectioning was carried out by mechanically breaking each target; the sectioned surface then observed directly with no further preparation[1] using a JEOL–JSM 6360 SEM. In selected cases, X-ray photoelectron spectroscopy was also used to study changes in the surface properties. XPS spectra are acquired using a PHI XPS system with a Mg Kα X-ray source and a detector pass energy of 25 eV with the binding-energy calibration conducted utilizing vacuum-deposited Au and Cu specimens and assigning the Au (4f7/2) and Cu (2p3/2) peaks values of 83.9 eV and 932.5 eV respectively [19]. Heat treatment/annealing was performed on selected targets using a vacuum furnace to study the thermal/mechanical stability of surface nanostructure at temperatures at, and in excess of, its formation temperature.

3. Results

We begin a description of the results with an analysis of mass change on targets due to plasma exposure. Fig. 1 shows the mass change of each target, Δm, plotted as a function of the He^+ ion fluence received during exposure. These data represent collectively all of the 24 exposed targets. To plot the data in this way, it must be noted that individual plasma exposure conditions for each target were not consistent. However, while a wide range of plasma–target conditions are evident, it can be noted that the energy of bombarding He ions was controlled and within the range 25–60 eV; that is, below the threshold for physical sputtering by either He or D. It can also be remarked that all of the targets were observed to have formed He-induced-nanostructured surfaces and that sputtering of W should not be expected to cause weight loss or morphology changes in this energy range. This is in fact confirmed by Fig. 1. The mass change data reveal that W-nanostructured layers do not erode, in agreement with TRIM calculations [20], nor detach or peel to result in increased mass loss at higher He^+ ion fluence. This can be concluded from the weighted-linear fit to the data (full line), which within uncertainty limits (dashed lines) has a slope and intercept that encompasses zero.

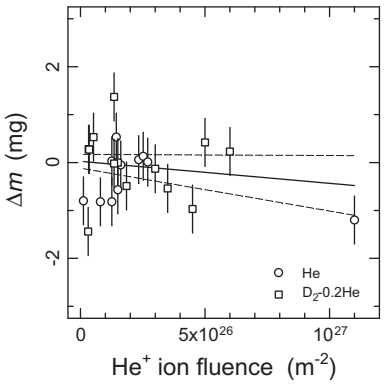

Fig. 1. Mass change, Δm, on W targets following exposure to pure He or D_2–0.2He mixture plasmas, plotted as a function of He^+ ion fluence received during exposure.

In Fig. 2, the dependence of nanostructure formation on exposure temperature is explored. The SEM cross-sections of three pure W targets are shown for pure He plasma exposure conditions of ~1 h at 900 K, 1120 K and 1320 K. The images reveal that increased temperature promotes an increased rate of surface transformation into thicker nanostructured layers. Interestingly, below 900 K, nanostructured layers are not observed after a full 1 h of plasma exposure. However, it is pointed out that a recent transmission electron microscopy (TEM) analysis [21] of a W target exposed to pure He plasma for ~1 h at 573 K in PISCES-A, revealed an extensive sub-surface plethora of nanoscopic bubbles in close proximately to the near surface (100–200 nm deep). It is probable that such features exist also in the 900 K exposed target of Fig. 2a, but are not resolvable by conventional SEM.

In Fig. 3, W 4f XPS spectra are compared. Data are shown for a polished-W target that was not exposed to plasma, in contrast with that of a nanostructured-W surface produced by 1 h of pure He plasma exposure at 1120 K, ($E_{He+} \sim 30$ eV). For the unexposed target, the 4f peaks at 31.0 eV and 33.5 eV are in good agreement with accepted values [19] for pure W, but there is also evidence of smaller shifted 4f peaks (~36 eV and 38 eV) that can be associated with a ~20% coverage of the surface with O, bound in the form WO_3. For the nanostructured surface (examined in situ after He plasma exposure), the XPS spectrum shows little evidence of any oxide, and while the usual W 4f peaks are also un-shifted, it is noted that a reduced photoelectron count by ~60% is evident. It can be inferred, from the lack of any shift in the 4f peaks, that nanostructured-W surfaces are not induced by impurity binding or any notable transformation of the W lattice. The noted reduction in peak height is explainable due to changes in the surface morphology caused by nanostructure growth: That is, X-rays that illuminate deeper parts of the nanostructured layer will produce photoelectrons that have a reduced probability for escape, and so detected photoelectron count is lower. This reduced photoelectron

[1] The usual preparative steps for SEM (e.g. – mounting, section polishing, C or Au conductive film deposition) grossly alter the appearance of surface nanofeatures and are not employed here.

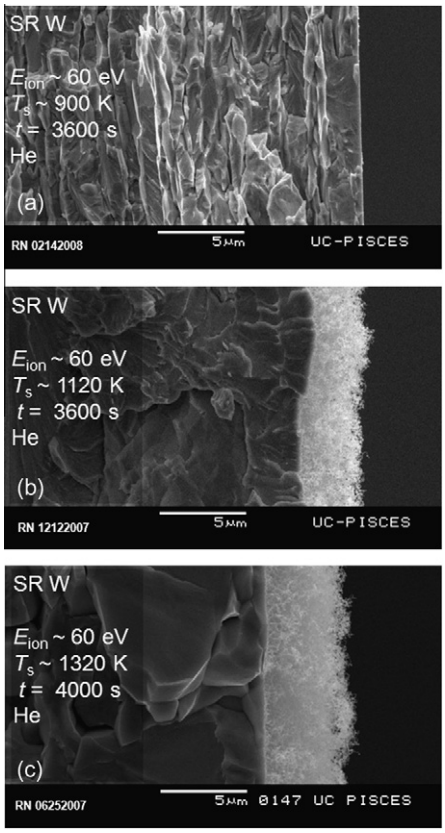

Fig. 2. Cross-sectional SEM micrographs of W targets exposed at (a) 900 K, (b) 1120 K, and (c) 1320 K to pure He plasma for ~1 h.

count points to the fact that a nanostructured surface layer is significantly porous compared to pure W.

The porosity of a nanostructured layer was estimated by taking advantage of the fact that such a layer can be removed easily from a target surface by wiping it. This estimate is established by measuring the volume of the nanostructured layer with cross-sectional SEM, and measuring the associated weight change (loss) due to wipe removal of the layer. The porosity of the nanostructured layer is equivalent to the ratio of the overall density of the removed layer with that of pure W.[2] A pure W target with a nanostructured surface was prepared by exposure to pure He plasma at 1120 K for 1 h ($E_{He+} \sim 30$ eV). The target was cross-sectioned and profiled with SEM as shown in Fig. 4a. A layer of nanostructured W close to 3 μm thick was measured to be uniform across the target surface. Fig 4b and c show SEM cross-sections of the target, in precisely the same location before and after the target was wiped (wiping removes the nanostructured layer and restores the initial mirror finish because of the scale of nanoscopic features). The corresponding mass loss was measured to be 870 ± 40 μg for an established geometrical volume of $7.8 \pm 0.8 \times 10^{-10}$ m^3 of nanostructured layer. The corresponding density of the layer is thus 1115 ± 127 kg m^{-3}, which is only 5.8 ± 1.1% of the density of pure W (19,250 kg m^{-3}). That is, the nanostructured layer, in this case, was 94% unoccupied space.

In Fig. 5 the material dependent variability of the nanostructure growth process is examined for various grades of W relevant to fusion engineering practice. Nine different types of polished-W target were explored by exposure to pure He plasma at 1120 K for durations of 1 h under conditions of consistent He$^+$ impact energy ($E_{He+} \sim 40$ eV). Fig. 5, displays SEM cross-sections for the following W material types:

[2] Porosity measurement includes any internal nanobubble structure [14].

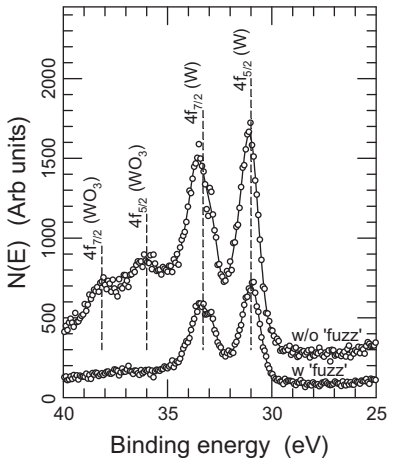

Fig. 3. W 4f X-ray photoelectron spectra for an unexposed W target and a W-nanostructured target produced by 1 h of pure He plasma exposure at 1120 K.

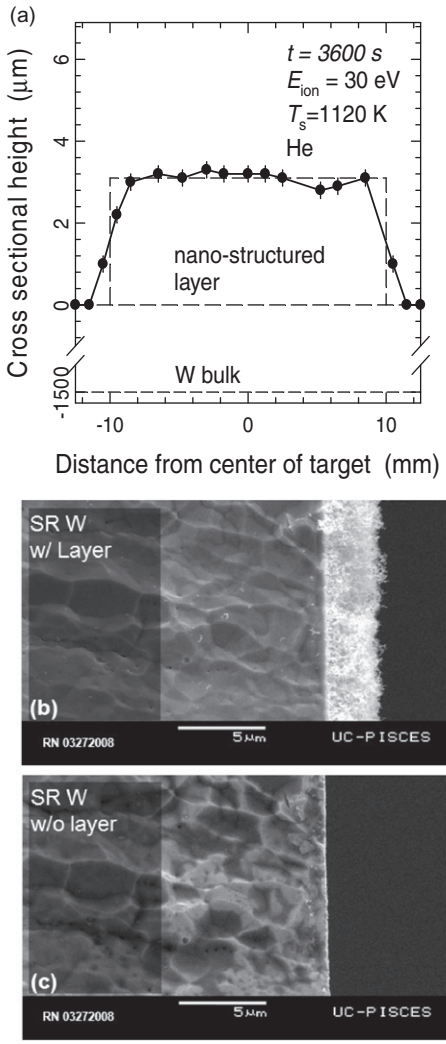

Fig. 4. (a) Nanostructure layer thickness profile measured with cross-sectional SEM for a W target exposed to pure He plasma at 1120 K for 1 h. Cross-sectional images (b) before, and (c) after wipe removal of the nanostructure layer.

(a) A 99.97% wt. rolled W target supplied by PLANSEE that was stress annealed at 1273 K for 1 h (considered the standard grade in this experiment).

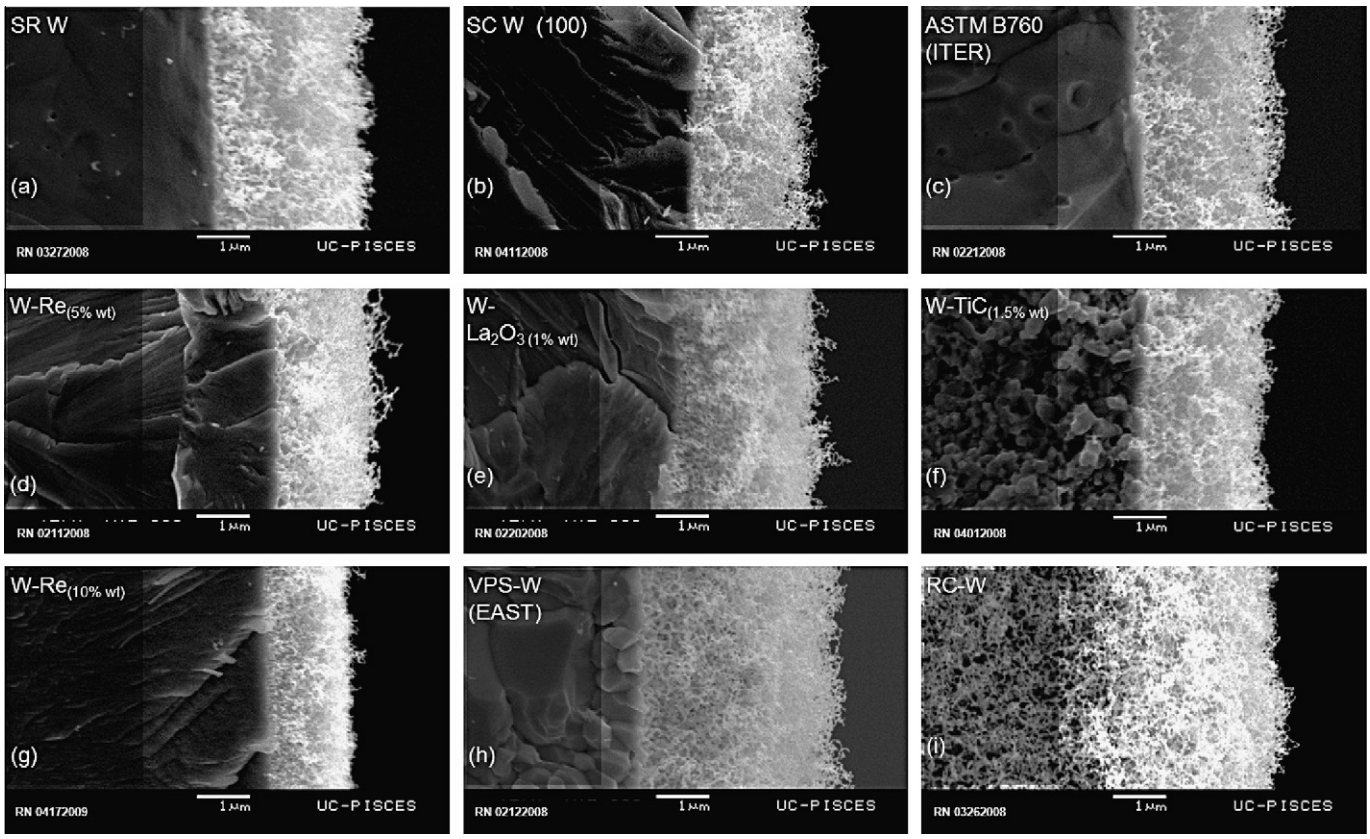

Fig. 5. Cross-sectional SEM images for nine different grades of W relevant to fusion engineering practice. All target specimens were exposed to consistent pure He plasmas at 1120 K for 1 h. The He^+ impact energy was ~40 eV. The following grades are explored: (a) PLANSEE SR W, (b) SC ⟨1 0 0⟩ W, (c) ITER ASTM B760 compliant W, (d) PLANSEE W–Re (5% wt.), (e) PLANSEE W–La_2O_3 (1% wt.), (f) UFG W–TiC (1.5% wt.), (g) ULTRAMET CVD W–Re (10% wt.), (h) VPS W (EAST) and (i) RC-W. Refer to text for description.

(b) A W ⟨1 0 0⟩ single crystal (SC) produced by the floating-zone-melting method (e.g. [2]).
(c) A W grade compliant with the ITER ASTM B760 standard. That is, grain orientation is normal to the surface and parallel to the incident heat flux.
(d) A W doped with Re (5% wt.) supplied by PLANSEE – USA.
(e) A W doped with La_2O_3 (1% wt.) supplied by PLANSEE – USA.
(f) An ultra fine grained (UFG) W doped with TiC (1.5% wt.) (as in Ref. [22]).
(g) A W sample produced by chemical vapor deposition (CVD) doped with Re (10% wt.) supplied by ULTRAMET–USA.
(h) A specimen of vacuum plasma sprayed (VPS) W of similar manufacturing method to VPS W components used in the EAST tokamak.
(i) And a W target produced by powder metallurgy methods but heat treated to above the recrystallization (RC) temperature (~1800 K).

All of the W grades explored showed the formation of a nanostructured layer between ~2 and 4 μm thick on the W target surface. The ITER compliant – Fig. 5c, SC – Fig. 5b, doped La_2O_3 (1% wt.) – Fig. 5e, and TiC (1.5% wt.) – Fig. 5f, grades developed nanostructured layers of thickness comparable to that observed on the standard rolled-pure W SR grade – Fig. 5a. The VPS (EAST) grade – Fig. 5h, developed the thickest nanostructured layer at almost 4 μm thick, while the Re doped PLANSEE (5% wt.) – Fig. 5d, and (10% wt.) – Fig. 5g, ULTRAMET CVD varieties showed the best resistance to nanostructure formation; both with nanostructured layers close to 2 μm in thickness. On the other hand, the RC-W target showed an extraordinary reaction to the He plasma, Fig. 5i, with findings different from the other grades, Fig. 5a–h.

Cross-sectional analysis of the He-plasma-exposed RC grade revealed the formation of nanostructuring at very deep locations when compared to the other targets. A selection of SEM images shows this in Fig. 6. The uppermost image, Fig. 6a, depicts a low-magnification view of the cross-section of this target. Images below show higher magnifications of the locations indicated 'A–D' – Fig. 6b–e respectively. The magnified location 'A' reveals the usual observation of a layer of nanostructure about 3 μm thick. However, evidence of nanostructuring is not limited to this layer, as it is with the other grades, of Fig. 5a–h. Nanostructuring can 'be observed many microns deeper. Regions 'B' and 'C', ~200–300 μm deep also show evidence af nanoscopic structuring. Only at depths almost 1000 μm deep do the nanoscopic features no longer appear, as in location 'D'. The presence of deep nanostructuring in the RC-W grade is almost certain to be a consequence, in some way, of the recrystallization process. During recrystallization, impurities, defects and vacancies proceed towards grain boundaries, to induce there a higher concentration of trapping sites. This higher proportion of available trapping sites, in turn, could lead to He bubble formation and ensuing nanostructure growth in grain boundary regions. Here it is worth mentioning that preferential He nanobubble growth at near surface W grain boundaries has been observed experimentally with TEM [23] on 8 keV He^+ irradiated W specimens at 1073 and 1273 K. In contrast to [23] however, the observations reported here are located very deep within the RC-W target. It is unclear why such deep nanostructuring should occur but not implausible since the rate of diffusion of He in W is known to be fast [24]; at 1123 K, the diffusion length is 2.07 cm after 3600 s, assuming that the temperature dependence of the diffusion coefficient quoted in [24] extrapolates accurately to high temperature >1000 K. A further comment is made pertain-

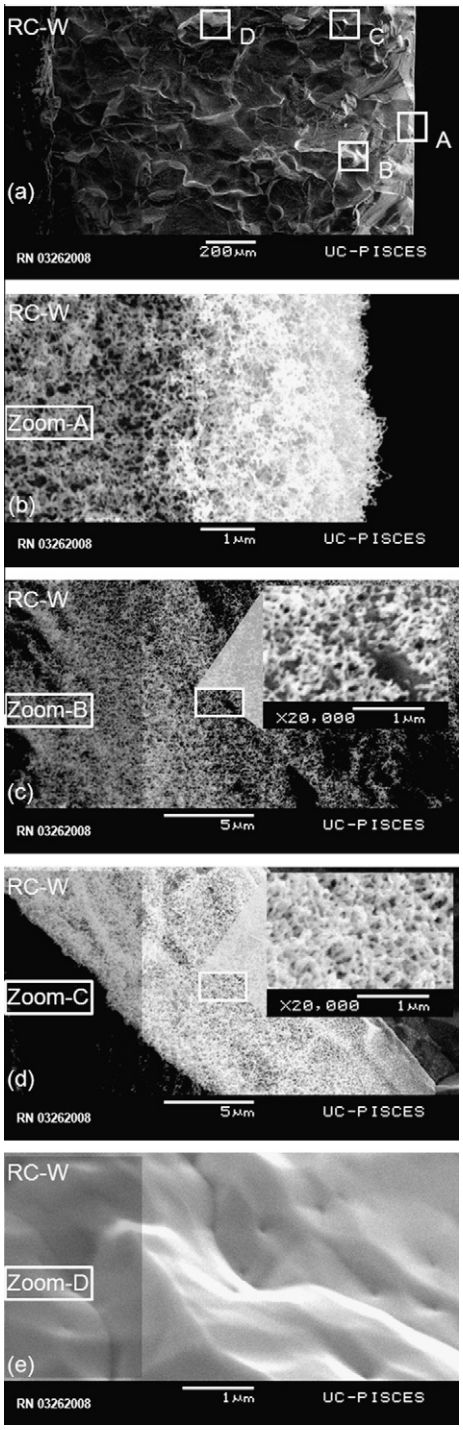

Fig. 6. Additional cross-sectional SEM analysis of the RC-W specimen of Fig. 5i. (a) Low magnification 'key' image. Boxes A–D are magnified in images (b–e). Refer to text for description.

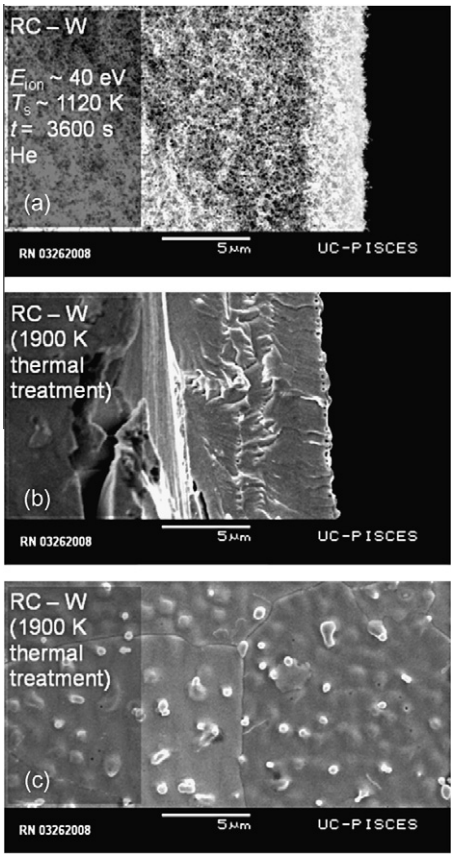

Fig. 7. SEM analysis of the RC-W target of Fig. 5i after heat treatment to 1900 K over 45 min. (a) Cross-section showing nanostructure formation. After heat treatment there is a reintegration of nanostructure with the bulk as shown by the (b) cross-section image and (c) surface image.

ing to the RC-W images of Fig. 5i and Fig. 6b–d. These images give the appearance that deep grains (unconnected with the surface) have transformed volumetrically into nanostructure similar to the surface layer. However, evidence of deep nanostructuring in these images must only be a transformation of the grain boundaries. For an entire grain to undergo transformation, an associated expansion in grain volume (by a factor of ~19, since nanostructure is porous) would be necessary to maintain a consistent number of W atoms in the grain. It is therefore believed, that the appearance of nanostructured grains reflects specimen preparation for cross-sectional SEM. Targets are broken by the application of shear stress when sectioned. Breakage ought to be preferential along grain boundaries that are weakened by nanostructure formation, and any boundary that is parallel to the break would therefore give the appearance of an entire grain conversion to nanostructure. The observation of deep nanostructure after just 1 h of plasma exposure, is nevertheless alarming. Grain-boundary embrittlement on such a reduced time scale, could place a limit on permissible W PFC temperature excursions/transients to below that necessary to cause recrystallization, and as such warrants further study.

A final study involved the examination of the resilience of nanostructured surfaces at high temperature using a vacuum furnace capable of reaching 2000 K. Selected pure W targets with nanostructured surface layers 2–3 μm thick, produced by exposure to pure He plasma for 1 h at 1120 K, were heat treated in-vacuo over periods of 45 min to maximum temperatures of 900 K, 1450 K and 1900 K. Target temperature was ramped linearly with time to its maximal value and the desorption of He monitored using a residual-gas analyzer. Fig. 7 shows a cross-section and surface-normal image of the RC-W target (Figs. 5i and 6) which was chosen for the heat treatment to 1900 K. In spite of the maximum temperature being well below the melting point for W, all traces of nanostructure, both surface and grain boundary, are found to be absent from the target following the heat treatment. Further, there is no convincing mass change observed after heat treatment, suggesting that nanostructures reintegrated with the W bulk. Only minor bubble formation, left at the very near surface suggests the presence of any He-induced effect. A similar result was also

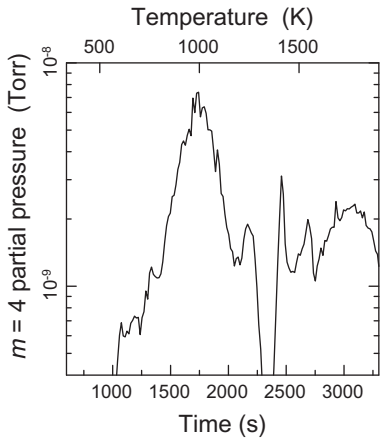

Fig. 8. He desorption profile for the RC-W target of Fig. 5i during heat treatment to 1900 K over 45 min.

found for the target heat treated to 1450 K, but the target heat treated to only 900 K retained its layer of surface nanostructure. These observations suggest that W mobility has a significant influence over the wide range of He-induced effects observed with temperature. Fig. 8 shows the release of He from the RC-W target of (Figs. 5i and 6) as it was heated to 1900 K. The data of Fig. 8 reveal a complex thermal-release spectrum broadly characterized by dominant release peaks at ~1000 K and ~1400–1800 K.

4. Discussion

Helium-induced-surface modification of W is caused by the action of He below the material surface, and the nature of formed surface features varies greatly with temperature. A substantial amount of work can be found in the available literature on He effects in metals, in general, but there are few accounts that describe the temperature window where the formation of He-induced-nanoscopic structure is known to occur. It is therefore appropriate to begin with a brief summary of previous findings relevant to the current study:

He on W induced nanostructuring is a visually black layer of modified W on the plasma interacting surface consisting of W 'branch' like structures, ~10–50 nm in thickness and of up to a micron in length [12–17]. Tokunaga et al. [12] first reported this surface blackening on pressed and plasma-sprayed-tungsten targets following exposure at 900 K[3] to 100 eV He^+ ions in PISCES-B. The blackening was determined to be W of sub-micron scale morphology with SEM and shown to be almost pure W with Auger electron spectroscopy. Takamura et al., observed similar morphology on tungsten coated graphite targets exposed to NAGDIS-II pure He plasmas at temperatures spanning 1250–1600 K [13] and was first to characterize its structure. In their article, a closer examination of the morphology than in [12], revealed that the tungsten surface was deeply nanostructured. The change in surface properties was brought about by the formation of a conglomerate of disordered 'nanorod' like structures, that were later confirmed by TEM analysis, to have internal nanometer sized bubbles or voids [14]. Article [13] demonstrated that such surface modification is produced in spite of the fact that incident He does not have sufficient energy to physically sputter or cause atomic displacement, although at least an incident He impact energy of ~20 eV is reported to be necessary to observe the effect [25].

[3] It is now known, that the singular temperature of 900 K, quoted in [12], is low by as much as 100–200 K because of a limitation of the temperature measurement system at that time.

Using the PISCES-B device, Baldwin and Doerner [15] explored the nature of nanostructured surface evolution over time. SEM cross-sectioning of targets exposed to He plasma for up to 2.2×10^4 s at 1120 K revealed that nanostructuring occurs over a volumetric surface layer, and that this layer is not limited to the near surface. The nanostructured layer was found to increase in thickness proportionately with the square root of the plasma exposure time and reached several microns in thickness in ~1 h. In a follow on study, Tokunaga et al. [16] showed this to be true also in more divertor relevant D_2–0.2He mixture plasmas used to expose TiC doped nanodispersoid W grades, and that the kinetics of the layer-growth are not significantly influenced by deuterium in the mixed-species plasma. The $t^{1/2}$ dependencies observed in [15,16] suggest that at least some part of the nanostructuring process is rate limited by a diffusive step, albeit this step remains unclear.

In another study [17], the dependence of the nanostructured layer thickness on He ion flux was established. For consistent plasma exposure times of 1 h at 1120 K, the layer-growth rate was found to be optimal provided that the incident He^+ bombardment flux was at or above 7×10^{21} m^{-2} s^{-1}. For He^+ fluxes below this value, the observed nanostructured layer thickness is exponentially reduced in thickness as He ion flux is reduced, suggesting a formation mechanism that relies on a high concentration of He in the W lattice. Ref. [17] further examined the influence of ITER relevant plasma impurities on nanostructure formation. It was shown that small amounts of Be and C plasma impurities (<1% n_e) can prevent the formation of nanostructuring under conditions where a protective-deposited layer can form on the target. However, it is unclear whether the deposited layer acts as a physical barrier to helium uptake, or whether the modified mixed-material surface structure was resilient to nanostructuring. Due to the high-exposure temperature (1150 K), the protective layers were noted to have chemically reacted with the W surface to form tungsten berryllides and carbides respectively. These results offered, at least, potential insight into how nanostructuring could be mitigated, but only under plasma conditions that did not contribute to the removal of the deposited mixed-material layer by sputtering. Where the deposited layer was sputter removed, a form of mixed-material nanostructuring was found with low level Be or C fractions.

In most previous studies of He-induced nanostructuring, the main focus is on the plasma conditions that lead to the effect and the influence that these conditions have on nanostructure growth. In this article, emphasis is given to examining the nature of the effect on the material. The mass change data of Fig. 1 reveal that W-nanostructured layers do not erode significantly under low-energy-plasma bombardment, nor detach by peeling or crumbling over exposure times up to 2.2×10^4 s. Yet such layers can be easily removed by light mechanical/abrasive action. In an ITER full-W-divertor scenario, we consider it possible that such nanostructure could form in locations where the correct formation conditions exist but little comment on the survivability of such surfaces can be made presently since reactor events such as ELMS and disruptions may adversely affect layer stability.

The results of Fig. 2 indicate that W-nanostructure-growth is more efficient as surface temperature is increased, but below 900 K nanostructuring is not found. At low-to-moderate temperature, up to 1000 K, ion-implanted He is known to induce surface blistering and subsequent exfoliation of blister caps [7,8] for W exposed to high-energy-particle beams. However, the blistering effect does not seem to manifest itself with W specimens exposed to low-energy He-plasma bombardment [21]. A few studies actually show a desirable He-induced effect in the low-to-moderate temperature range. He plasma pre-treatment [26] and He exposure in mixed-species D_2–He plasmas [21] has been shown to reduce hydrogen isotope retention and blistering. He-induced near surface

nanobubbles, confirmed by TEM, acted in some to way to prevent the uptake of hydrogen isotopes at the very near surface in those experiments. At higher temperature though (>1000 K), He inclusion in the W lattice produces dramatic changes to the surface. The He plasma exposures at 1120 K and 1320 K in Fig. 2b and c clearly reveal a layer of nanostructuring and the increased thickness of the layer with temperature points to the involvement of thermally-activated processes.

When considering Fig. 2, further insight into the nanostructure growth process is perhaps possible in light of other work found in the literature: TEM [21,23] and SEM [17] analyses. In [21], near surface He bubble formation was found on He-plasma-exposed W targets, but evidence of He-induced-nanoscopic morphology was not. The exposure temperature was only 573 K. In [23], TEM analysis of nanoscopic morphology formed at 1250 K showed that nanoscopic features also contain He nanobubbles. That is, near surface nanobubbles are common to both accounts, but nanostructuring only occurs at the highest temperatures. The difference points to the thermo-physics of the W material itself and suggests that nanobubbles, although necessary, do not entirely give rise to nanostructure formation. He-induced nanobubbles must be an active mechanism however, since W exposed to hydrogen isotope plasma at >1000 K [17] does not form surface nanobubbles and nanostructuring is not observed. Both nanobubbles and a high temperature ($0.25 < T/T_m < \sim 0.4$) seem to be necessary. There are many thermally-activated materials process that could play a role. W mobility, vacancy transport, adatom diffusion, bubble/cluster migration are all thermally-activated processes, to name a few (e.g. [27]), but it remains to be satisfactorily verified as to the precise manner in which all processes lead to formation of individual nanostructures. A heuristic description of nanostructure formation, based on experimental observation, is depicted in [25] showing bubble migration and coalescence as drivers of nanostructure growth. However, there is currently no He–W materials interaction modeling that demonstrates the outcome of a He-induced-W nanoscopic structure of any similarity to experiment.

The X-ray photoelectron analysis of Fig. 3 shows that W-nanostructure is a reorganization of the W surface. There is no evidence of chemical binding or altered structure; W-nanostructure is of similar material structure to that of the bulk, albeit nanoscopically deformed. In the target case of Fig. 4, the nanoscopic deformation was estimated to lead a value of porosity for the nanostructure layer that is extremely high; more than 90% of the layer is determined to be unoccupied space between interconnected nanoscopic structures and its internal bubble structure. It is presently unclear the effect that such porosity will have on the thermal properties of such surfaces and so research effort is currently underway in these laboratories to examine the impact of ELM like heat loads on nanoscopic structure using a pulsed-laser system.

When combined, the lack of any convincing mass loss due to plasma exposure (Fig. 1) and measurement of porosity (inferred from Fig. 4), have shed further light on the findings published in an earlier article [15]. In [15], nanostructured layers are shown to grow in thickness as the exposure time to He plasma is increased: In Fig. 3 of Ref. [15], cross-sectioned W targets with nanostructured layers are aligned adjacently so that the top of the layer is used as a common point of reference. While, visually, this demonstrated the growth in thickness of the nanostructured layer, it gives the unintended appearance that nanostructure grows into the W surface. To some extent this is true, but it is not a fully correct interpretation. The established measure of unoccupied space in a nanostructured layer (inferred from Fig. 4), and knowledge that nanoscopic layers do not erode significantly (Fig. 1) under the plasmas conditions explored here and also in [15], suggests that nanostructured layers in fact grow away from the W surface; consuming the W bulk to a depth of ~6% of the measured nanostructured layer thickness. A reduced selection of the images of Fig. 3 in [15] has been re-arranged in Fig. 9 to demonstrate this more accurate picture. The dashed lines depict the boundaries of the nanostructured layer while the full line, drawn across the image set, is a representation of where the original polished surface would have been located. As was reported in Ref. [15], the images in Fig. 9 depict a growth process whereby the thickness of the nanostructured layer, δ, grows proportionately with the plasma exposure time according to, $\Delta = \beta t^{1/2}$, where $\beta = 1.3 \times 10^{-15}\ m^2\ s^{-1}$ at 1120 K.

Mathematically, such a process sees the change of layer thickness as increasingly limited at large times compared to early stage growth, but in a fusion device, the survivability of thick nanostructured layers is questionable. Should nanostructured layers be easily removed in an actual fusion environment, it is the re-growth rate, $d\Delta/dt = \beta/(2t^{1/2})$ that is alarming. In a balanced equilibrium between simultaneous nanostructure growth and removal (e.g. ablation, ELMS, etc.), to leave only a reduced layer thickness δ, the re-growth rate is $(d\Delta/dt)_{\Delta=\delta} = \beta^2/(2\delta)$. That is, continual removal of the layer to a reduced thickness, promotes increasingly rapid material loss depending on the smallness of δ, and whether such equilibrium can be maintained. Further experiments, to test for such enhanced material loss, are currently underway in the PISCES laboratory, but a true test can only really be assessed in an actual fusion device.

The efficiency of nanostructure formation in pure He plasma is explored in Fig. 5 for nine different varieties of W relevant to fusion-reactor construction. The images of Fig. 5 show that none of the explored pure or doped varieties are resilient to the formation of nanostructuring. Small levels of the dopants Re (5% wt.), La_2O_3 (1% wt.) and TiC (1.5% wt.) produce little effect on the rate of nanostructure growth, and it is found that W material grades, where trap concentrations (vacancies, defects, voids) are expected to be higher (VPS and RC grade grain boundaries) develop the highest rates of nanostructure formation. Yet, any pre-existing trap concentration must act in addition to other He-trapping mechanisms. This is because even SC W readily succumbs to surface nanostructuring, producing a nanostructure layer of comparable thickness to the other W grades. This surprising result suggests that nanostructuring is related to a He-trapping mechanism that is self driven, since the natural concentration of vacancies and defects in SC W should be very low and the thermal vacancy fraction at 1120 K is exceptionally small ($V_c = 5.22 \times 10^{-12}$, e.g. Ref. [28]). Self-driven trapping has been studied for some time. In one account, proposed by Wilson, Bisson and Baskes [29] it was shown that small localizations of as few as five interstitial He atoms lead to a large enough distortion of the W matrix to produce a lattice vacancy and self interstitial pair. Further, in their calculations, a cluster of 8 or 16 He atoms leads to 2 or 5 such pairs. In this view, He clustering followed by the production and saturation of He traps, precursor to He bubbles and nanostructuring, should depend on the He concentration in the lattice, or alternatively the incident energetic He flux to the surface. Interestingly, the dependence of nanostructuring on He ion flux was observed in Ref. [17].

In Fig. 5, the only target explored that seemingly showed any resilience to nanostructuring was the CVD target containing 10% wt. Re and a systematic trend can be observed by comparing the images Fig. 5a 0% wt. Re, Fig. 5d 5% wt. Re, and Fig. 5g 10% wt. Re, respectively. Each of these targets was produced by a different manufacturing method, which complicates interpretation, but the trend suggests that an increased level of alloy content is a method for reducing the efficiency of nanostructuring. Full alloying, such as in [17], where target surfaces were layers of the mixed-materials Be_{12}–W and WC were noted to be fully resistant to nanostructuring, but these particular mixed-materials present other intrinsic issues in a fusion environment.

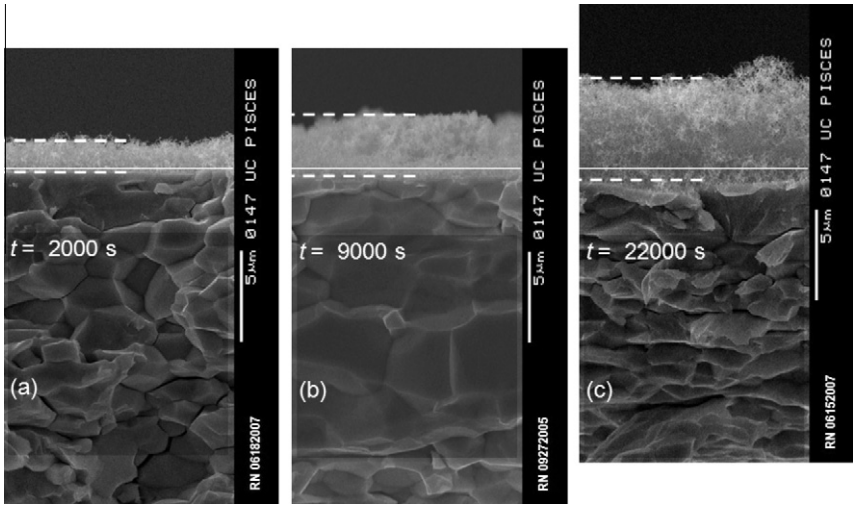

Fig. 9. Reduced selection of cross-sectional SEM images of Fig. 3 in Ref. [15] demonstrating outward growth of nanostructure from the target surface. Targets are PLANSEE SR W exposed to pure He plasma for exposures times of (a) 2.0×10^3 s, (b) 9.0×10^3 s and (c) 2.2×10^4 s at 1120 K. The dashed lines depict the boundaries of the nanostructured layer. The full line, drawn across the image set, is a representation of where the original polished surface would have been located.

The images of Fig. 7 demonstrate the mobility of W at temperatures well below its melting point. All traces of nanostructure at surface and grain boundary locations on the RC-W target are removed after only 1 h of thermal treatment to 1900 K, and the absence of any convincing mass change suggests a reintegration of nanostructure and W bulk. Interestingly, He is released from the target at temperatures both below, and much in excess, of the formation temperature of the nanostructured surface, as in Fig. 8, indicating release properties whereby He is highly mobile yet also strongly bound to trapping mechanisms. Kornelsen and Van Gorkum have studied He desorption from W extensively [30]. By comparison with their work, the major release peaks of Fig. 9 (~1000 K and ~1400–1800 K) could be associated with He desorption form highly decorated and degenerate He–vacancy complexes.

5. Conclusions

A wide variety of W material grades (SR, SC, weakly doped (Re, La_2O_3, TiC), VPS, ASTM B760 (ITER) and RC) relevant to fusion engineering practice are found to develop nanostructured surface layers when exposed to pure He or fusion relevant D_2–0.2He mixture plasmas in the PISCES-B linear divertor-plasma simulator, when operated at ITER/DEMO relevant temperatures of 900–1320 K. A layer of nanoscopically reorganized W, between 2 and 4 μm thick is found on all target specimens explored. Reorganization is thought to occur because of the combined effects of nanoscopic bubble formation and increased W mobility with temperature. In the case of RC-W, nanostructuring was found at deep (up to several hundred μm) locations after just 1 h of plasma exposure, presenting reduced time scale grain-boundary embrittlement issues. When growth conditions are met, nanostructuring occurs for incident He^+ ion fluences of impact energy (25–60 eV) well below that required for the sputtering of W by He and, in a fusion scenario, could present a source of fragile, high–Z material at the plasma edge that continuously grows away from the W PFC surface. A nanostructured layer, measured for its porosity was found to be at least 90% unoccupied space, but survived without detachment, peeling or crumbling for up 2.2×10^4 s in the PISCES-B plasma environment. However, layer survivability in an actual fusion device requires further study to examine the additional influences of ELMS and disruptions. He-induced-nanostructuring of W surfaces has been observed in a wide variety of plasma devices under an equally wide range of plasma conditions. Surface modification has been reported on W targets exposed to energetic helium in PISCES-B [12,15–17], PISCES-A, NAGDIS-II [13,14,21 and Refs. therein], LHD [31], a low-pressure Rf plasma device [17], the GLADIS device at IPP Garching [18] and also on W components in an inertial electrostatic confinement (IEC) device at the Univ. of Wisconsin [32]. Thus, He-induced W nanostructuring is seemingly device independent and is a materials issue driven by the action and accumulation of He in the elevated temperature W matrix. Presently, heavy alloying, for example with Re as shown here, or with incident plasma impurity species (e.g. Be or C as in Ref. [17]) are known to reduce/mitigate the nanostructuring effect, but other strategies must also be developed.

Acknowledgements

The authors wish to acknowledge the skill and dedication of Pisces-B technical staff and Beryllium Enclosure personnel, particulary T. Lynch and R Seraydarian. The authors further wish to thank, Dr. K. Schmid of the Max-Planck Institut für Plasmaphysik, Dr. L. Guangnan of the Institute of Plasma Physics, Chinese Academy of Sciences, Dr. K. Tokunaga of the Kyushu University & Mr M. Wright of ULTRAMET–USA for the donation of W target materials. This work is supported by the US–EU Collaboration on Mixed-Materials, the US–JAPAN 'TITAN' collaboration and US–DOE: Grant Award #DE-FG02-07ER54912.

References

[1] J.N. Brooks, J.P. Allain, R.P. Doerner, A. Hassanein, R. Nygren, T.D. Rognlien, D.G. Whyte, Nucl. Fusion 49 (2009) 035007.
[2] K. Tokunaga, M.J. Baldwin, R.P. Doerner, N. Noda, Y. Kubota, N. Yoshida, T. Sogabe, T. Kato, B. Schedler, J. Nucl. Mater. 337–339 (2005) 887.
[3] R.P. Doerner, M.J. Baldwin, G. De Temmerman, J. Hanna, D. Nishijima, J. Roth, K. Schmid, G.R. Tynan, K. Umstadter, Nucl. Fusion 49 (2009) 035002.
[4] L.K. Keys, J.P. Smith, J. Moteff, Phys. Rev. 176 (1968) 851.
[5] F. Najmabadi et al., Fusion Eng. Des. 80 (2006) 3.
[6] N. Noda, V. Philipps, R. Neuc, J. Nucl. Mater. 241–243 (1997) 227.
[7] S. Nagata, B. Tsuchiya, T. Sugawara, N. Ohtsu, T. Shikama, J. Nucl. Mater. 307–311 (2002) 1513.
[8] K. Tokunaga, S. Tamura, N. Yoshida, K. Ezato, M. Taniguchi, K. Sato, S. Suzuki, M. Akiba, J. Nucl. Mater. 329–333 (2004) 757.
[9] D. Nishijima, M.Y. Ye, N. Ohno, S. Takamura, J. Nucl. Mater. 313–316 (2003) 97.
[10] M.Y. Ye, H. Kanehara, S. Fukuta, N. Ohno, S. Takamura, J. Nucl. Mater. 313–316 (2003) 72.
[11] D. Nishijima, M.Y. Ye, N. Ohno, S. Takamura, J. Nucl. Mater. 329–333 (2004) 1029.

[12] K. Tokunaga, R.P. Doerner, R. Seraydarian, N. Noda, Y. Kubota, N. Yoshida, T. Sogabe, T. Kato, B. Schedler, J. Nucl. Mater. 313–316 (2003) 92.
[13] S. Takamura, N. Ohno, D. Nishijima, S. Kajita, Plasma Fusion Res. 51 (2006) 1.
[14] N. Yoshida, H. Iwakiri, Damage structure of tungsten under He particle loading, in: Proc. 1st Int. Symposium and 1st Korea–Japan Workshop on Edge Plasma and Surface Component Interactions in Steady State Magnetic Fusion Devices, Toki, Japan, 20–22 May 2007.
[15] M.J. Baldwin, R.P. Doerner, Nucl. Fusion 48 (2008) 035001.
[16] K. Tokunaga, M.J. Baldwin, R.P. Doerner, D. Nishijima, H. Kurishita, T. Fujiwara, K. Araki, Y. Miyamoto, N. Yoshida, N. Ohno, Y. Ueda, Nanoscopic morphology formation on tungsten induced by D–He mixture plasma exposure, in: 25th Symposium on Fusion Technology, Rostock, Germany, 15–19 September 2008.
[17] M.J. Baldwin, R.P. Doerner, D. Nishijima, K. Tokunaga, Y. Ueda, J. Nucl. Mater. 390–391 (2009) 886.
[18] H Maier, H Greuner et al., personal communication.
[19] C.D. Wagner, W.M. Riggs, L.E. Davis, J.F. Moulder, G.E. Mullenberg, Handbook of X-ray Photoelectron Spectroscopy, Published by Perkin-Elmer Corp., Eden Prairie, MN, USA, 1979.
[20] W. Eckstein, IPP Report 9/17, 1998.
[21] M. Miyamoto, D. Nishijima, Y. Ueda, R.P. Doerner, H. Kurishita, M.J. Baldwin, S. Morito, K. Ono, J. Hanna, Nucl. Fusion 49 (6) (2009) 065035.
[22] H. Kurishita, S. Matsuo, H. Arakawa, S. Kobayashi, K. Nakai, T. Takida, K. Takebe, M. Kawai, Mater. Sci. Eng. A 477 (1–2) (2008) 162.
[23] N. Yoshida, in: Proc. 1st Int. Symposium and 1st Korea–Japan Workshop on Edge Plasma and Surface Component Interactions in Steady State Magnetic Fusion Devices, Toki, Japan, 20–22 May 2007.
[24] J. Amano, D.N. Seidman, J. Appl. Phys. 56 (1984) 983.
[25] S. Kajita, W. Sakaguchi, N. Ohno, N. Yoshida, T. Saeki, Nucl. Fusion 49 (2009) 095005.
[26] D. Nishijima, H. Iwakiri, K. Amano, M.Y. Ye, N. Ohno, K. Tokunaga, N. Yoshida, S. Takamura, Nucl. Fusion 45 (2005) 669.
[27] F.P. Bowden, K.E. Singer, Nature 222 (1969) 977.
[28] E. Lassner, W.D. Schubert, Tungsten: Properties, Chemistry, Technology of the Element, Alloys and Chemical Compounds, Kluwer Academic/Plenum Publishers, New York, 1999.
[29] W.D. Wilson, C.L. Bisson, M.I. Baskes, Phys. Rev. B. 24 (1981) 5616.
[30] E.V. Kornelsen, A.A. Van Gorkum, J. Nucl. Mater. 92 (1980) 79.
[31] M. Tokitani, M. Miyamoto, D. Koga, K. Tokunaga, T. Fujiwara, N. Yoshida, S. Masuzaki, N. Ashikawa, T. Morisaki, M. Shoji, A. Komori, J. Nucl. Mater. 337–339 (2005) 937.
[32] S. Zenobia, R.F. Radel, B.B. Cipiti, G.L. Kulcinski, J. Nucl. Mater. 389 (2009) 213.